

Constraining early dark energy with gravitational waves before recombination

Zachary J. Weiner,^{1,*} Peter Adshead,^{1,†} and John T. Giblin, Jr.^{2,3,‡}

¹*Illinois Center for Advanced Studies of the Universe & Department of Physics,
University of Illinois at Urbana-Champaign, Urbana, Illinois 61801, USA*

²*Department of Physics, Kenyon College, Gambier, Ohio 43022, USA*

³*CERCA/ISO, Department of Physics, Case Western Reserve University, Cleveland, Ohio 44106, USA*

We show that the nonperturbative decay of ultralight scalars into Abelian gauge bosons, recently proposed as a possible solution to the Hubble tension, produces a stochastic background of gravitational waves which is constrained by the cosmic microwave background. We simulate the full nonlinear dynamics of resonant dark photon production and the associated gravitational wave production, finding the signals to exceed constraints for the entire parameter space we consider. Our findings suggest that gravitational wave production from the decay of early dark energy may provide a unique probe of these models.

I. INTRODUCTION

Measurements of the current expansion rate H_0 as inferred from the acoustic peaks in the cosmic microwave background (CMB) radiation are in tension with the value obtained from local measurements [1–3], suggesting the need to extend the concordance Λ cold dark matter cosmological model. Rather than alter the expansion history at intermediate redshifts, new physics introduced to resolve the tension must alter the absolute scales of the low- or high-redshift anchors of the cosmic distance scale [4, 5]. Early-Universe resolutions thus focus on altering the high-redshift anchor, the CMB sound horizon at recombination. For a recent review, see Ref. [6].

In particular, an increased expansion rate before recombination decreases the sound horizon. However, simply adding more radiation [7, 8] also changes the damping scale in a way that is increasingly disfavored by high-precision measurements of the high-multipole damping tail [2, 9, 10]. To avoid this, one class of proposed solutions, so-called early dark energy (EDE) models, postulates an additional energy component that is only transiently important near recombination [11–20]. These proposed solutions supposedly relieve the tension between the early and late data sets; however, see Refs. [21, 22].

In the simplest EDE implementations, a scalar field is initially frozen up its potential in a homogeneous configuration. The field’s mass is tuned such that it begins to evolve near matter-radiation equality, oscillating about the minimum of its potential. In order to redshift away fast enough (at least as fast as radiation), the potential must have no quadratic term about its minima. From a particle physics perspective, this requires an explanation; to avoid such extreme fine-tuning, Ref. [18] instead proposed a model of a *decaying* ultralight scalar (dULS). Instead of oscillating about a peculiar potential and redshifting away, the EDE scalar field decays resonantly

to dark radiation during oscillations about a quadratic minimum.

Nonperturbative or resonant particle production is a common feature of early-Universe preheating after inflation (for reviews, see Refs. [23–25]). Substantial study has established that these violent processes can also lead to the copious production of gravitational waves [26–41]. The wavelength of the produced gravitational waves (GWs) is determined by the characteristic scale of particle production, which must be smaller than the horizon size. During preheating after inflation this restricts the production to frequencies from MHz to GHz, well beyond the reach of current or planned detectors [42–48].¹ By contrast, in order to resolve the Hubble tension, particle production due to the decay of the ultralight scalar must occur near the time of matter-radiation equality. Since resonant particle production occurs at scales near the horizon scale at that time, gravitational wave emission occurs at current-day frequencies near 10^{-16} Hz. CMB anisotropies constrain stochastic gravitational waves with peak sensitivity at present-day frequencies near 10^{-17} Hz [51, 53–55]. In this paper, we confront models of ultralight scalar decay into dark photons with these constraints.

II. BACKGROUND

Following Ref. [18], we study the resonant decay of an ultralight axion ϕ into a (dark) Abelian gauge field A_μ described by the action

$$S = \int d^4x \sqrt{-g} \left[\frac{M_{\text{Pl}}^2}{2} R - \frac{1}{2} \partial_\mu \phi \partial^\mu \phi - V(\phi) - \frac{1}{4} F_{\mu\nu} F^{\mu\nu} - \frac{\alpha}{4f} \phi F_{\mu\nu} \tilde{F}^{\mu\nu} \right]. \quad (1)$$

¹ However, high-frequency gravitational waves contribute to the energy budget of the Universe as radiation. Constraints on the gravitational-wave energy density from N_{eff} [49–52] can be used to indirectly restrict preheating scenarios [39–41].

* zweiner2@illinois.edu

† adshead@illinois.edu

‡ giblinj@kenyon.edu

Here f is the axion decay constant and α is a dimensionless coupling that parametrizes the rate and efficiency of energy transfer. The field-strength tensor of the dark photon is $F_{\mu\nu} \equiv \partial_\mu A_\nu - \partial_\nu A_\mu$, while its dual is $\tilde{F}^{\mu\nu} = \epsilon^{\mu\nu\alpha\beta} F_{\alpha\beta}/2$, where $\epsilon^{\mu\nu\rho\sigma}$ is the Levi-Civita symbol with convention $\epsilon^{0123} = 1/\sqrt{-g}$. Following Ref. [18], we take the standard axion potential $V(\phi) = m_\phi^2 f^2 (1 - \cos \phi/f)$. We set $c = \hbar = k_B = 1$ and use $M_{\text{pl}} = 1/\sqrt{8\pi G_N}$ to denote the reduced Planck mass. We work with the ‘‘mostly plus,’’ conformal Friedmann-Lemaître-Robertson-Walker (FLRW) metric, $g_{\mu\nu} = a^2 \eta_{\mu\nu} = a^2 \text{diag}(-1, 1, 1, 1)$, using primes to denote derivatives with respect to conformal time τ .

The classical equations of motion,

$$A_\nu'' = \partial_i \partial_i A_\nu + \eta_{\beta\nu} \frac{\alpha}{f} \partial_\alpha \phi \left(\frac{1}{2} \sqrt{-g} \epsilon^{\alpha\beta\rho\sigma} F_{\rho\sigma} \right) \quad (2)$$

$$\phi'' = \partial_i \partial_i \phi - 2\mathcal{H}\phi' - a^2 \frac{dV}{d\phi} - a^2 \frac{\alpha}{4f} F_{\mu\nu} \tilde{F}^{\mu\nu}, \quad (3)$$

permit solutions in which fluctuations of the gauge fields are exponentially enhanced via a tachyonic instability sourced by a homogeneous, rolling axion. Initially, a cosmological axion has some static homogeneous component $\langle \phi \rangle = \theta f$, expressed in terms of the initial misalignment angle θ . As a result, the axion’s energy is dominated by its potential, acting as a source of early dark energy which could alleviate the Hubble tension [13]. On the other hand, to linear order the helical polarizations of A_i obey [56]

$$A_\pm''(\mathbf{k}) + k \left(k \mp \frac{\alpha}{f} \langle \phi' \rangle \right) A_\pm(\mathbf{k}) = 0. \quad (4)$$

Thus, once the axion begins to oscillate (when the Hubble parameter drops below $\sim m_\phi/3$ [57]), its non-negligible background velocity causes one of the two polarizations to undergo tachyonic resonance, i.e., to be amplified exponentially for modes $k < \alpha/f \times \langle \phi' \rangle$.

As the axion crosses zero, $\langle \phi' \rangle$ changes sign and so amplifies the other polarization. Eventually, the gauge field fluctuations become so large that nonlinear effects begin to fragment the axion background, ending the phase of tachyonic resonance. Both the initial exponential gauge field production and subsequent nonlinear dynamics can source a significant gravitational wave background. Gravitational waves correspond to the tensor part of perturbations to the spatial part of the spacetime metric,

$$h_{ij}'' - \partial_k \partial_k h_{ij} + 2\mathcal{H}h_{ij}' = \frac{2}{M_{\text{pl}}^2} T_{ij}^{\text{TT}}, \quad (5)$$

where T_{ij}^{TT} is the transverse and traceless part of the stress-energy tensor T_{ij} .

We employ numerical simulations in order to fully capture resonance, the nonlinear dynamics which terminate energy transfer, and the resulting production of gravitational waves. We solve the classical equations of motion

Eqs. (2), (3), and (5) in a homogeneous Λ CDM cosmology, self-consistently including the contribution of the dULS sector to the expansion rate. We discretize these equations onto a three-dimensional, periodic, regularly spaced grid, computing spatial derivatives via fourth-order centered differencing and utilizing a fourth-order Runge-Kutta method for time integration. All results presented use grids with $N^3 = 768^3$ points, side length $L = 10/m_\phi$, and a time step $\Delta\tau = \Delta x/10 = L/10N$. We implement simulations using `pystella` [40, 41] and provide details on our algorithm, initial conditions, and convergence tests in the Appendices.

III. RESULTS

In our simulations of the decaying ultralight scalar model, we consider benchmark scenarios from Ref. [18], taking $m_\phi = 10^{-27} - 10^{-26}$ eV so that the dULS sector transitions from dark energy to matter-like behavior around the favored redshift $z_c \approx 16500$. Because the axion begins to oscillate when $H \sim m_\phi$, its relative contribution to the Universe’s energy scales as $\rho_\phi/\rho \sim m_\phi^2 (\theta f)^2 / H^2 \sim (\theta f)^2$, independent of m_ϕ . Thus, we set $f = 1.5 \times 10^{17}$ GeV (and an initial misalignment angle $\theta = 2$ for convenience) so that the dULS sector makes up $\sim 3 - 4\%$ of the Universe’s energy budget at its peak. We comment later on the dependence of the gravitational wave signal on slight changes in these choices.

We first verify that the dynamics of the dULS sector qualitatively reproduce the effective fluid description employed in Ref. [18] (which we evaluate in more detail in Appendix C). In Fig. 1 we display the energy in the gauge fields ρ_A and the fractional energy in the dULS sector, $\Omega_{\text{dULS}} = (\rho_A + \rho_\phi)/\rho$, as a function of redshift. We vary the coupling α from 50 to 70, spanning values large enough for resonance and GW production to terminate before recombination while small enough to be reliably resolved by our grid.

Figure 2 depicts the gravitational wave signal resulting from the resonant production of dark photons, evaluated at $z = 1100$. We compare the signal to the constraints from a recent analysis of current data in Ref. [54].² While the peak of the fractional gravitational wave energy spectrum (reaching above 10^{-11}) resides at larger frequencies $\sim 10^{-14}$ Hz, the infrared tail of the spectrum exceeds constraints at frequencies $\lesssim 10^{-16}$ Hz by roughly an order of magnitude. We note that, though we are unable to simulate larger volumes to capture even lower frequencies,

² Note that the constraints of Ref. [54] are not directly applicable to this scenario, since they are computed from adiabatic initial conditions—constant initial GW amplitude on superhorizon scales. By contrast, the GWs here are actively sourced, analogous to those in defect scenarios, e.g., Ref. [58]. However, we expect constraints on active modes to be competitive, if not more severe than those on adiabatic modes.

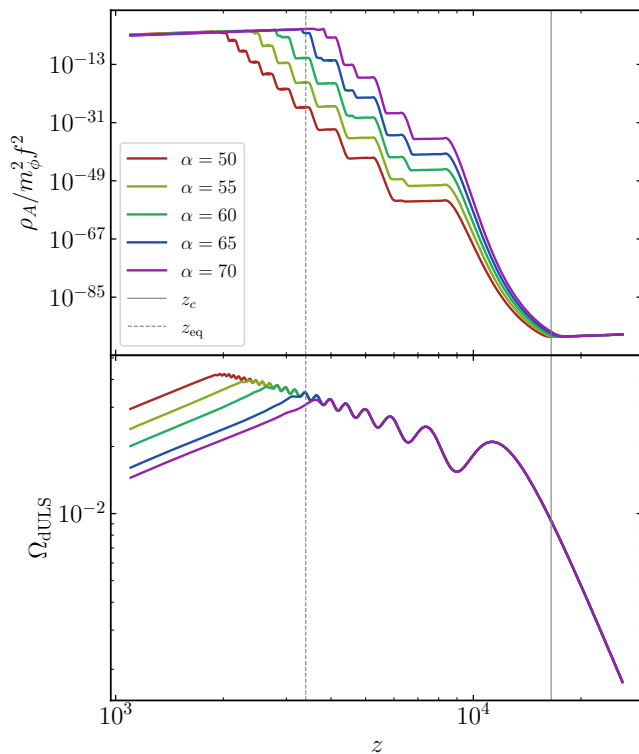


FIG. 1. Total energy in the gauge fields (top) and the fractional energy in the dULS sector (bottom) as a function of redshift for various couplings α indicated in the legend. All simulations fix $m_\phi = 10^{-26}$ eV, $f = 1.5 \times 10^{17}$ GeV, and $\theta = 2$. Dashed and solid vertical lines indicate, respectively, matter-radiation equality and the favored redshift of the transition from dark energy to matter from the analysis of Ref. [18].

we expect the signal should continue roughly as a power law further into the infrared, $\Omega_{\text{gw}} \propto k/k_*$, where k_* is the peak wave number, as suggested by recent analytic estimates of GW production in similar scenarios [59].

The analysis of Ref. [18] determined that the dULS sector should begin to decay like radiation by a redshift between ~ 11000 and 5000 ; as a result, if this scenario is to alleviate the Hubble tension, the associated gravitational wave signal will be produced before recombination, $z \approx 1400 - 1100$ [53]. While the couplings we are able to study here only probe transitions to radiation-like behavior at the later end of this interval, our findings offer no reason to expect the signal from models with larger couplings to evade CMB constraints.

We now consider the dependence of gravitational wave production on other model parameters. The scaling of the signal with the axion mass m_ϕ is relatively simple. From the transfer function (derived in Appendix A), the present-day frequency scales as $f \sim k/\sqrt{HM_{\text{pl}}} \sim \sqrt{m_\phi/M_{\text{pl}}}$. While the axion mass scales out of the dynamics, it has an effect on the initial amplitude of gauge field vacuum fluctuations. A lower mass sets initial fluctuations with lower amplitude, requiring a longer period of resonance

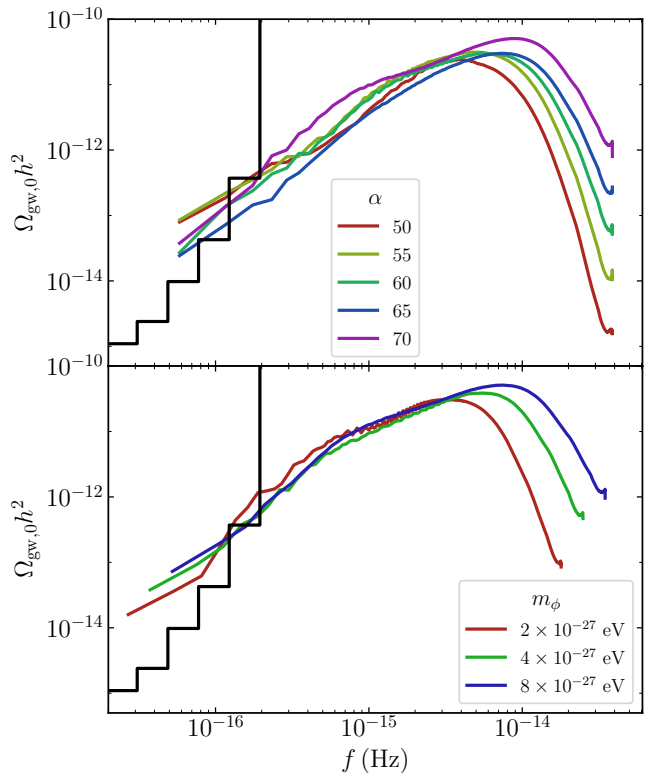


FIG. 2. Present-day gravitational wave spectrum emitted by recombination (i.e., evaluated at $z \approx 1100$), fixing $m_\phi = 10^{-26}$ eV and varying α (top) and fixing $\alpha = 70$ and varying m_ϕ (bottom). All simulations set $f = 1.5 \times 10^{17}$ GeV and $\theta = 2$. In black is the upper bound as constrained by the CMB, computed in Ref. [54].

to fully deplete the axion's energy. However, this effect is relatively unimportant and is easily compensated for by a slight increase in the coupling α . At smaller masses, resonance begins later; therefore, marginally larger couplings are required in order for the process to complete before recombination (so that the signals are detectable). As can be seen in the bottom panel of Fig. 2, this condition is easily met with $\alpha = 70$ and a variety of masses between 10^{-27} and 10^{-26} eV. Furthermore, the shape and amplitude of the GW signal itself is qualitatively independent of the axion mass m_ϕ .

The value of the axion decay constant f is set by the requirement that the dULS sector comprises a fraction of the Universe's energy between $3 - 4\%$, leaving little room for variation. Namely, at the onset of oscillations, the fractional energy in the axion scales as $\rho_\phi/\rho \sim m_\phi^2(\theta f)^2/H^2 \sim (\theta f)^2$. In turn, the amplitude of the resulting gravitational wave signal is directly proportional to the square of the fraction of the Universe's energy residing in its source [60]. Since the signals we find here exceed current constraints by an order of magnitude, we do not expect the constraining power of the GW signal to be sensitive to any uncertainty in the best-fit ρ_ϕ/ρ .

Since θ sets the amplitude of axion oscillations (and

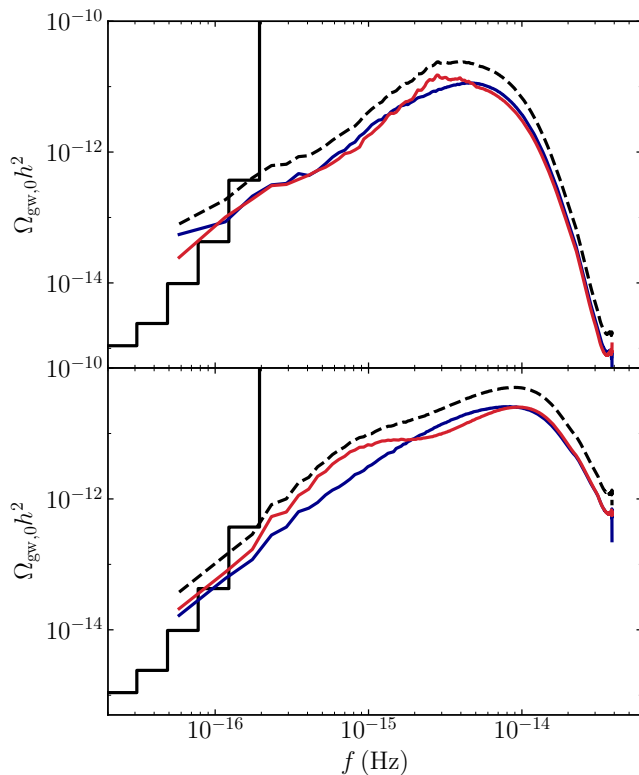


FIG. 3. Polarization components of the present-day gravitational wave spectrum emitted by recombination (i.e., evaluated at $z \approx 1100$) for $\alpha = 50$ (top) and 70 (bottom). The plus and minus polarizations are in blue and red, respectively, while the total signal is portrayed in dashed black. Both panels fix $m_\phi = 10^{-26}$ eV, $f = 1.5 \times 10^{17}$ GeV, and $\theta = 2$. In solid black is the upper bound as constrained by the CMB, computed in Ref. [54].

so $\langle \phi' \rangle$, its effect on the dynamics is, to linear order, degenerate with the coupling. However, nonlinear effects (e.g., rescattering of power to higher momenta) become more important with larger couplings α , and so our choice of $\theta = 2$ allows reliable simulations with smaller couplings that still transition the dULS sector to a radiation-like state on the required time scales.

As a final investigation, we study whether the gravitational wave signal is significantly polarized. The same axial coupling of gauge fields to the inflaton generates a helical gravitational wave background during inflation [61–65], and can also imprint on the spectrum of gravitational waves produced during preheating [39]. However, in the former case, the sign of the axion’s velocity is fixed during inflation. Preheating via the axial coupling can also complete within one (or even half an) oscillation of the inflaton [40, 41, 56], but nonlinear effects can result in a gravitational wave signal dominated by different helicities at different scales. The results presented in Fig. 3 follow in spirit. For the lowest coupling we consider, $\alpha = 50$, the axion oscillates numerous times before gauge field production terminates, emitting an essentially unpolarized

gravitational wave background. For the largest coupling, $\alpha = 70$, the spectrum is moderately polarized at large scales, consistent with a more substantial enhancement of one polarization before the axion first crosses zero. While the signal at lower frequencies arises predominantly from the initial phase of helical tachyonic resonance, higher frequencies are sourced by nonlinear mode interactions which do not retain the same polarization. In summary, it is difficult to evaluate whether the gravitational wave background is sufficiently polarized on CMB scales to provide a unique signature of this model; doing so likely requires thorough study via numerical simulations in a model-dependent way. As an aside, we note that these findings are applicable to models of dark matter as massive dark photons, which are produced via the same resonant instability considered here [66–71].

IV. CONCLUSIONS

The rapid production of inhomogeneities from resonant particle production can induce a significant GW background. The amplitude of the GW signal is largest (and so offers the most constraining potential) when the GW source comprises a significant fraction of the Universe’s energy budget and occurs close to the horizon scale at the time of emission [60]. The model considered here, which exhibits a tachyonic instability via an axion coupled to dark photons, is especially efficient, as has been shown in the context of preheating after inflation [40, 41] in which case up to the entire energy budget of the Universe may source gravitational waves. New physics which relies on the same mechanism later in cosmological history is subject to constraints from direct probes of stochastic backgrounds of gravitational waves [51, 53]. Models of early dark energy proposed to alleviate the Hubble tension are a prime example, as their success hinges on the new sector making up a substantial [$\mathcal{O}(1\%)$] fraction of the Universe’s energy. Furthermore, the source of early dark energy must soon decay one way or another before recombination, pinning the relevant length scales to those probed by the cosmic microwave background.

In this work, we demonstrated that the decaying ultralight scalar model, as motivated in Ref. [18], produces a background of gravitational waves with a peak spectral energy fraction exceeding $\mathcal{O}(10^{-11})$ at its peak, with a power-law tail extending into the region that is already constrained by the CMB [54]. While we have not studied the entire available parameter space, we showed that the requirements for the model to successfully alleviate the Hubble tension generally coincide with those for its gravitational wave signature to be constrained by the CMB. For the parameter space we considered, we found that the signal exceeds constraints (on adiabatic modes) by an order of magnitude. Because GWs are actively sourced in this scenario, these constraints are not directly applicable, and we leave a detailed computation of the CMB signatures of these models to future work. However,

we expect the importance of this differing time dependence to be suppressed: in terms of line-of-sight solutions, the contribution of tensors to the CMB is weighted by the visibility function, which is sharply peaked at the time of recombination [72]. In addition, recent work has proposed spectral distortions as a probe of gravitational waves at higher frequencies than those directly probed by the CMB [73], which would be sensitive to the peak of the signals presented here.

Finally, we point out that resonant particle production is not a unique feature of this model. The original single-field models of EDE exhibit similar parametric instabilities which may also emit significant GW backgrounds [15]. More broadly, our findings suggest that stochastic backgrounds of gravitational waves could provide an orthogonal probe with which to constrain models of early dark energy.

ACKNOWLEDGMENTS

We gratefully acknowledge Tom Clarke, Ed Copeland, and Adam Moss for sharing the data from Ref. [54], and we thank Tristan Smith for useful discussions. The work of P.A. was supported in part by NASA Astrophysics Theory Grant NNX17AG48G. J.T.G. is supported by the National Science Foundation Grant No. PHY-1719652. Z.J.W. is supported in part by the United States Department of Energy Computational Science Graduate Fellowship, provided under Grant No. DE-FG02-97ER25308. This work used the Extreme Science and Engineering Discovery Environment (XSEDE) [74], which is supported by National Science Foundation grant number ACI-1548562; simulations were run on the Comet cluster at the San Diego Supercomputer Center through allocation TG-PHY180049. This work made use of the Illinois Campus Cluster, a computing resource that is operated by the Illinois Campus Cluster Program (ICCP) in conjunction with the National Center for Supercomputing Applications (NCSA) and which is supported by funds from the University of Illinois at Urbana-Champaign.

Simulations in this work were implemented with `pystella`, which is available at github.com/zachjweiner/pystella and makes use of the Python packages `PyOpenCL` [75], `Loo.py` [76], `mpi4py` [77, 78], `mpi4py-fft` [79], `NumPy` [80], and `SciPy` [81].

Appendix A: Equations and numerical implementation

The dynamical system, our conventions, and our numerical implementation match those of Refs. [40, 41] (see the appendices of Ref. [40] for full details), with relatively minimal differences we describe here.

The energy density and pressure which source FLRW expansion comprise contributions from the standard background Λ CDM model, the axion, and the gauge fields.

The spatially-averaged energy density and pressure are

$$\rho_\phi(\tau) \equiv \left\langle \frac{\phi'^2}{2a^2} + \frac{(\partial_i \phi)^2}{2a^2} + V(\phi) \right\rangle, \quad (\text{A1})$$

$$p_\phi(\tau) \equiv \left\langle \frac{\phi'^2}{2a^2} - \frac{(\partial_i \phi)^2}{6a^2} - V(\phi) \right\rangle \quad (\text{A2})$$

for the axion and

$$\rho_A(\tau) \equiv \frac{1}{2} \langle \mathbf{E}^2 + \mathbf{B}^2 \rangle, \quad (\text{A3})$$

$$p_A(\tau) \equiv \frac{1}{6} \langle \mathbf{E}^2 + \mathbf{B}^2 \rangle \quad (\text{A4})$$

for the gauge fields. Above we defined the electric and magnetic fields

$$E_i = \frac{1}{a^2} (A_i' - \partial_i A_0), \quad B_i = \frac{1}{a^2} \epsilon_{ijk} \partial_j A_k. \quad (\text{A5})$$

In our simulations, we consistently include the contributions of Eqs. (A1) to (A4) to the expansion rate alongside the background Λ CDM model.

The axion–dark-photon coupling violates parity and so the resonantly produced gauge bosons are helical (at least initially), which may in principle imprint on the resulting gravitational waves. For details on the decomposition of gravitational waves into the polarization basis, see Ref. [39].

The present-day spectrum $\Omega_{\text{gw}}(a_0)$ is related to that at the time of emission, $\Omega_{\text{gw}}(a_e)$, via

$$\frac{\Omega_{\text{gw}}(a_0)}{\Omega_{\text{gw}}(a_e)} = \left(\frac{a_e}{a_0} \right)^4 \frac{\rho(a_e)}{\rho(a_0)}, \quad (\text{A6})$$

since gravitational waves redshift like radiation. In turn, the present-day frequency of observation is determined from the physical momentum $k_{\text{phys}} = k/a_0$ via

$$f = \frac{k_{\text{phys}}}{2\pi} = \frac{1}{2\pi} \frac{k}{a_e} \frac{a_e}{a_0}. \quad (\text{A7})$$

The entropy of the Standard Model (SM) provides a conserved quantity by which we may compute a_e/a_0 at any time after the SM thermalizes. The entropy density is $s = 2\pi^2 g_{\star S}(T) T^3/45$, where T is the SM temperature and $g_{\star S}$ the number of effective degrees of freedom in entropy. Combining with $\rho_{\text{rad}} = \pi^2 g_{\star}(T) T^4/30$ (where g_{\star} is the effective number of degrees of freedom in energy density) allows one to express a_e/a_0 in terms of the energy density in radiation, g_{\star} , and $g_{\star S}$. Approximating $g_{\star S} = g_{\star}$ allows us to evaluate Eq. (A6) at any point after thermalization as

$$\Omega_{\text{gw}}(a_0) h^2 = \frac{\Omega_{\text{rad}}(a_0) h^2}{\Omega_{\text{rad}}(a_e)} \left(\frac{g_{\star}(a_0)}{g_{\star}(a_e)} \right)^{1/3} \Omega_{\text{gw}}(a_e). \quad (\text{A8})$$

Likewise, Eq. (A7) may be expressed as

$$f = \frac{k/2\pi a_e}{\sqrt{H(a_e) M_{\text{pl}}}} \left(\frac{\Omega_{\text{rad}}(a_0)}{\Omega_{\text{rad}}(a_e)} H_0^2 M_{\text{pl}}^2 \right)^{1/4} \left(\frac{g_{\star}(a_0)}{g_{\star}(a_e)} \right)^{1/12}. \quad (\text{A9})$$

While in general g_* may be evaluated using, e.g., tabulated values from Ref. [82], the effective number of relativistic degrees of freedom is fixed to 3.36 since well before the time of our simulations. The present radiation fraction $\Omega_{\text{rad}}(a_0)h^2 \approx 4.2 \times 10^{-5}$, and the radiation fraction at the time of emission is calculated during the simulation. Plugging in $H_0 = h \cdot 3.2 \times 10^{-18}$ Hz and $M_{\text{pl}} = 3.7 \times 10^{42}$ Hz,

$$f = \frac{k/a_e}{\sqrt{H(a_e)M_{\text{pl}}}} \Omega_{\text{rad}}(a_e)^{1/4} \times 4.33 \times 10^{10} \text{ Hz.} \quad (\text{A10})$$

To set initial conditions, we begin by solving for the dynamics of the linearized system. We evolve the Friedmann equations, the homogeneous and linear-order parts of the axion's equation of motion,

$$\langle \phi'' \rangle = -2\mathcal{H} \langle \phi' \rangle - a^2 \frac{dV}{d\langle \phi \rangle} - a^2 \frac{\alpha}{4f} \langle F_{\mu\nu} \tilde{F}^{\mu\nu} \rangle, \quad (\text{A11})$$

$$\delta\phi''(k) = -2\mathcal{H}\delta\phi'(k) - \left(k^2 + a^2 \frac{d^2V}{d\langle \phi \rangle^2} \right) \delta\phi'(k), \quad (\text{A12})$$

and the linearized equation of motion for the gauge field polarizations,

$$A_{\pm}''(\mathbf{k}) = -k \left(k \mp \frac{\alpha}{f} \langle \phi' \rangle \right) A_{\pm}(\mathbf{k}). \quad (\text{A13})$$

While solving the linearized system, we compute the gauge field contributions to the background dynamics by integrating over the evolved gauge field modes via numerical quadrature (as employed in Ref. [40]). We neglect the backreaction of the gauge fields onto the axion fluctuations in Eq. (A12), which is negligible even well after we initialize the full lattice simulation.

We begin the linear evolution when $H \gg m_{\phi}$ (so that all modes are far outside the horizon) and set $\langle \phi \rangle = \theta f$ and $\langle \phi' \rangle = 0$. The gauge fields are initialized in the Bunch-Davies vacuum,

$$\langle |A_{\pm}(\mathbf{k})|^2 \rangle = \frac{1}{2\sqrt{k}}, \quad (\text{A14})$$

$$\langle |A'_{\pm}(\mathbf{k})|^2 \rangle = \frac{\sqrt{k}}{2}. \quad (\text{A15})$$

The axion acquires a nearly scale-invariant spectrum of fluctuations during inflation,

$$\langle |\phi(\mathbf{k})|^2 \rangle = \frac{1}{k^3} \frac{H_{\text{inf}}^2}{2\pi^2}, \quad (\text{A16})$$

and $\delta\phi' = 0$. As a benchmark value, we take the inflationary Hubble scale $H_{\text{inf}} = 2 \times 10^9$ GeV, but our main results are insensitive to whether the axion is even initialized with any fluctuations.

We evolve the linear system until $H = m_{\phi}$, at which point we initialize the lattice simulation. The subsequent

dynamics are identical to when the lattice simulation is initialized when $H = 10m_{\phi}$, and are relatively unchanged even if initialized at $H = m_{\phi}/10$. Using the background values and power spectra obtained at this point ($H = m_{\phi}$), we initialize the lattice simulation with the procedure described in Ref. [40]. Our simulations use a grid with $N^3 = 768^3$ points and conformal box length $L = 10/m_{\phi}$, with a time step $\Delta\tau = \Delta x/10 = L/10N$. Though our computational resources only allowed for a single simulation (i.e., random realization of the initial conditions) per set of model parameters, we do not expect an ensemble average to exhibit significant variance in, e.g., the gravitational wave spectrum.

Appendix B: Convergence tests

The simulations we present in the main text require fairly large volumes to capture the IR tail of the gravitational wave spectrum which resides at CMB frequencies, while also sufficient resolution to capture both the initial tachyonic resonance band and the subsequent power transfer to higher momenta via nonlinear effects. As $N^3 = 768^3$ represents the largest grid size possible with our current resources, in lieu of an ideal convergence test (fixing the box length L while increasing N) we compare results for two box lengths, both with $N = 768$. We present this comparison for $L = 10/m_{\phi}$ (as used for main results) and $L = 5/m_{\phi}$ in Fig. 4, for $\alpha = 70$ (the largest coupling for which we present results, which should require the most resolution). Specifically, Fig. 4 depicts for each field the final dimensionless power spectra, i.e., for a field f ,

$$\Delta_f(k)^2 = \frac{1}{2\pi^2} \frac{1}{V} \int \frac{d\Omega}{4\pi} k^3 |f(\mathbf{k})|^2. \quad (\text{B1})$$

The results show excellent consistency, with expected discrepancy at the largest scales in the simulation (due to statistical variance) and negligible differences at the Nyquist frequency.

Appendix C: Comparing to the two-fluid description

We now compare the results of the full numerical simulation, the numerical solution to the linearized system, and the two-fluid model detailed in Ref. [18]. The latter is described by the effective fluid equations

$$\rho'_{\phi} + 3aH(1 + w_{\phi})\rho_{\phi} = -a\Gamma(\tau)\rho_{\phi}, \quad (\text{C1})$$

$$\rho'_A + 4aH\rho_A = a\Gamma(\tau)\rho_{\phi}, \quad (\text{C2})$$

where the axion equation of state is

$$w_{\phi}(a) = -1 + \frac{1}{1 + (a_c/a(\tau))^3} \quad (\text{C3})$$

and the decay rate is parameterized by

$$\Gamma(\tau) = \frac{m_{\phi}}{1 + (a_r/a(\tau))^p} \quad (\text{C4})$$

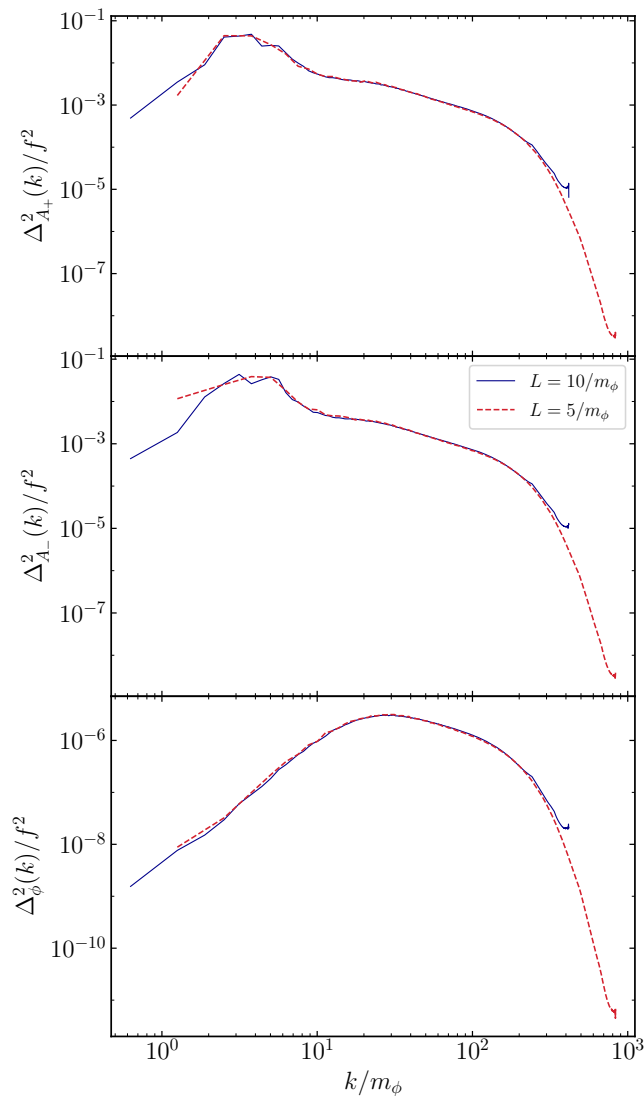


FIG. 4. Dimensionless power spectra of A_+ , A_- and ϕ (from top to bottom), evaluated at the end of the simulation ($z = 1100$), defined by Eq. (B1). All simulations fix $\alpha = 70$, $m_\phi = 10^{-26}$ eV, $f = 1.5 \times 10^{17}$ GeV, and $\theta = 2$. We compare simulations with box lengths $L = 10/m_\phi$ in solid, thin blue and $L = 5/m_\phi$ in dashed red.

with $p = 30$. In this effective description, the scalar field begins to oscillate at a_c , while the dULS sector transitions to radiation domination at a_r . We display the evolution of ρ_ϕ and ρ_A in Fig. 5. Qualitatively, the two-fluid model reproduces the energy transfer, but cannot account for the remnant energy remaining in the axion after resonance. This remaining energy is due to nonlinear effects preventing the axion condensate from being totally depleted as well as backreaction effects producing axion particles. In addition, Fig. 5 demonstrates the validity of the solution to the linearized system of equations in the early stages of resonance while also exhibiting the importance of nonlinear effects as resonance terminates.

-
- [1] A. G. Riess, S. Casertano, W. Yuan, L. M. Macri, and D. Scolnic, *Astrophys. J.* **876**, 85 (2019), [arXiv:1903.07603 \[astro-ph.CO\]](#).
- [2] N. Aghanim *et al.* (Planck), (2018), [arXiv:1807.06209 \[astro-ph.CO\]](#).
- [3] W. L. Freedman, *Nature Astron.* **1**, 0121 (2017), [arXiv:1706.02739 \[astro-ph.CO\]](#).
- [4] J. L. Bernal, L. Verde, and A. G. Riess, *JCAP* **10**, 019 (2016), [arXiv:1607.05617 \[astro-ph.CO\]](#).
- [5] K. Aylor, M. Joy, L. Knox, M. Millea, S. Raghunathan, and W. K. Wu, *Astrophys. J.* **874**, 4 (2019), [arXiv:1811.00537 \[astro-ph.CO\]](#).
- [6] L. Knox and M. Millea, *Phys. Rev. D* **101**, 043533 (2020), [arXiv:1908.03663 \[astro-ph.CO\]](#).
- [7] M. Wyman, D. H. Rudd, R. Vanderveld, and W. Hu, *Phys. Rev. Lett.* **112**, 051302 (2014), [arXiv:1307.7715 \[astro-ph.CO\]](#).
- [8] C. Dvorkin, M. Wyman, D. H. Rudd, and W. Hu, *Phys. Rev. D* **90**, 083503 (2014), [arXiv:1403.8049 \[astro-ph.CO\]](#).
- [9] W. Hu and M. J. White, *Astrophys. J.* **471**, 30 (1996), [arXiv:astro-ph/9602019](#).
- [10] M. Raveri, W. Hu, T. Hoffman, and L.-T. Wang, *Phys. Rev. D* **96**, 103501 (2017), [arXiv:1709.04877 \[astro-ph.CO\]](#).

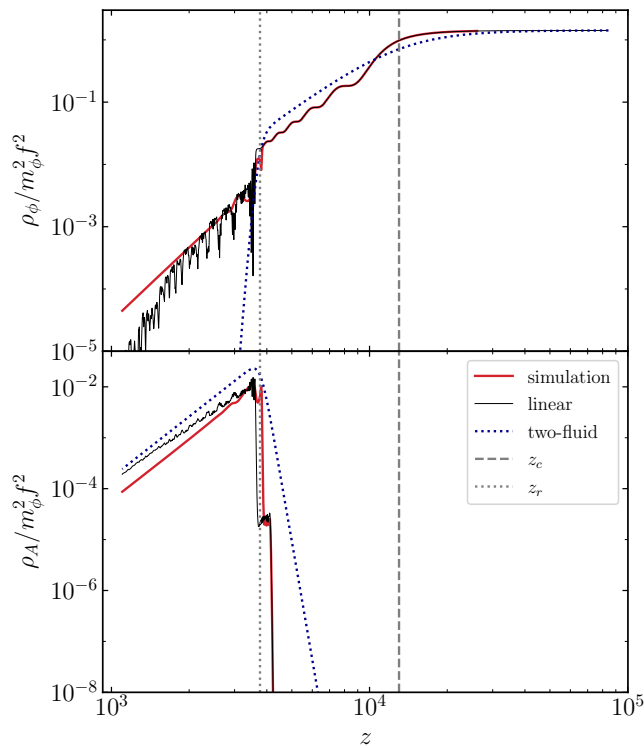


FIG. 5. Comparing numerical solutions for the full nonlinear system of equations (red), the linearized system (thin black), and the effective two-fluid description of Ref. [18] (dotted blue). Vertical lines denote the redshift of oscillation $z_c = a_0/a_c - 1$ (dashed grey) and that of the transition to radiation domination $z_r = a_0/a_r - 1$ (dotted grey). For the fluid model, we choose $a_c = 6.5$, $a_r = 3.5a_c$ to be consistent with the dynamics of the simulation and linear solution, which take $m_\phi = 10^{-26}$ eV, $\theta = 2$, $\alpha = 70$, and $f = 1.5 \times 10^{17}$ GeV.

- [11] T. Karwal and M. Kamionkowski, *Phys. Rev. D* **94**, 103523 (2016), [arXiv:1608.01309 \[astro-ph.CO\]](#).
- [12] V. Poulin, T. L. Smith, D. Grin, T. Karwal, and M. Kamionkowski, *Phys. Rev. D* **98**, 083525 (2018), [arXiv:1806.10608 \[astro-ph.CO\]](#).
- [13] V. Poulin, T. L. Smith, T. Karwal, and M. Kamionkowski, *Phys. Rev. Lett.* **122**, 221301 (2019), [arXiv:1811.04083 \[astro-ph.CO\]](#).
- [14] M.-X. Lin, G. Benevento, W. Hu, and M. Raveri, *Phys. Rev. D* **100**, 063542 (2019), [arXiv:1905.12618 \[astro-ph.CO\]](#).
- [15] T. L. Smith, V. Poulin, and M. A. Amin, *Phys. Rev. D* **101**, 063523 (2020), [arXiv:1908.06995 \[astro-ph.CO\]](#).
- [16] K. V. Berghaus and T. Karwal, *Phys. Rev. D* **101**, 083537 (2020), [arXiv:1911.06281 \[astro-ph.CO\]](#).
- [17] M. Braglia, W. T. Emond, F. Finelli, A. E. Gumrukcuoglu, and K. Koyama, (2020), [arXiv:2005.14053 \[astro-ph.CO\]](#).
- [18] M. Gonzalez, M. P. Hertzberg, and F. Rompineve, (2020), [arXiv:2006.13959 \[astro-ph.CO\]](#).
- [19] F. Niedermann and M. S. Sloth, (2019), [arXiv:1910.10739 \[astro-ph.CO\]](#).
- [20] F. Niedermann and M. S. Sloth, (2020), [arXiv:2006.06686 \[astro-ph.CO\]](#).
- [21] C. Krishnan, E. O. Colgáin, Ruchika, A. A. Sen, M. Sheikh-Jabbari, and T. Yang, (2020), [arXiv:2002.06044 \[astro-ph.CO\]](#).
- [22] J. C. Hill, E. McDonough, M. W. Toomey, and S. Alexander, *Phys. Rev. D* **102**, 043507 (2020), [arXiv:2003.07355 \[astro-ph.CO\]](#).
- [23] R. Allahverdi, R. Brandenberger, F.-Y. Cyr-Racine, and A. Mazumdar, *Ann. Rev. Nucl. Part. Sci.* **60**, 27 (2010), [arXiv:1001.2600 \[hep-th\]](#).
- [24] M. A. Amin, M. P. Hertzberg, D. I. Kaiser, and J. Karouby, *Int. J. Mod. Phys. D* **24**, 1530003 (2014), [arXiv:1410.3808 \[hep-ph\]](#).
- [25] K. D. Lozanov, (2019), [arXiv:1907.04402 \[astro-ph.CO\]](#).
- [26] S. Khlebnikov and I. Tkachev, *Phys. Rev. D* **56**, 653 (1997), [arXiv:hep-ph/9701423](#).
- [27] R. Easther and E. A. Lim, *JCAP* **04**, 010 (2006), [arXiv:astro-ph/0601617](#).
- [28] R. Easther, J. Giblin, John T., and E. A. Lim, *Phys. Rev. Lett.* **99**, 221301 (2007), [arXiv:astro-ph/0612294](#).
- [29] R. Easther, J. T. Giblin, and E. A. Lim, *Phys. Rev. D* **77**, 103519 (2008), [arXiv:0712.2991 \[astro-ph\]](#).
- [30] J. Garcia-Bellido and D. G. Figueroa, *Phys. Rev. Lett.* **98**, 061302 (2007), [arXiv:astro-ph/0701014](#).
- [31] J. F. Dufaux, A. Bergman, G. N. Felder, L. Kofman, and J.-P. Uzan, *Phys. Rev. D* **76**, 123517 (2007), [arXiv:0707.0875 \[astro-ph\]](#).
- [32] J.-F. Dufaux, D. G. Figueroa, and J. Garcia-Bellido, *Phys. Rev. D* **82**, 083518 (2010), [arXiv:1006.0217 \[astro-ph.CO\]](#).
- [33] L. Bethke, D. G. Figueroa, and A. Rajantie, *Phys. Rev. Lett.* **111**, 011301 (2013), [arXiv:1304.2657 \[astro-ph.CO\]](#).
- [34] D. G. Figueroa and T. Meriniemi, *JHEP* **10**, 101 (2013), [arXiv:1306.6911 \[astro-ph.CO\]](#).
- [35] L. Bethke, D. G. Figueroa, and A. Rajantie, *JCAP* **06**, 047 (2014), [arXiv:1309.1148 \[astro-ph.CO\]](#).
- [36] D. G. Figueroa, J. García-Bellido, and F. Torrentí, *Phys. Rev. D* **93**, 103521 (2016), [arXiv:1602.03085 \[astro-ph.CO\]](#).
- [37] D. G. Figueroa and F. Torrenti, *JCAP* **10**, 057 (2017), [arXiv:1707.04533 \[astro-ph.CO\]](#).
- [38] M. A. Amin, J. Braden, E. J. Copeland, J. T. Giblin, C. Solorio, Z. J. Weiner, and S.-Y. Zhou, *Phys. Rev. D* **98**, 024040 (2018), [arXiv:1803.08047 \[astro-ph.CO\]](#).
- [39] P. Adshead, J. T. Giblin, and Z. J. Weiner, *Phys. Rev. D* **98**, 043525 (2018), [arXiv:1805.04550 \[astro-ph.CO\]](#).
- [40] P. Adshead, J. T. Giblin, M. Pieroni, and Z. J. Weiner, *Phys. Rev. D* **101**, 083534 (2020), [arXiv:1909.12842 \[astro-ph.CO\]](#).
- [41] P. Adshead, J. T. Giblin, M. Pieroni, and Z. J. Weiner, *Phys. Rev. Lett.* **124**, 171301 (2020), [arXiv:1909.12843 \[astro-ph.CO\]](#).
- [42] J. Aasi *et al.* (LIGO Scientific), *Class. Quant. Grav.* **32**, 074001 (2015), [arXiv:1411.4547 \[gr-qc\]](#).
- [43] F. Acernese *et al.* (VIRGO), *Class. Quant. Grav.* **32**, 024001 (2015), [arXiv:1408.3978 \[gr-qc\]](#).
- [44] K. Somiya (KAGRA), *Class. Quant. Grav.* **29**, 124007 (2012), [arXiv:1111.7185 \[gr-qc\]](#).
- [45] P. Amaro-Seoane *et al.* (LISA), (2017), [arXiv:1702.00786 \[astro-ph.IM\]](#).
- [46] M. Punturo *et al.*, *Class. Quant. Grav.* **27**, 194002 (2010).
- [47] N. Seto, S. Kawamura, and T. Nakamura, *Phys. Rev. Lett.* **87**, 221103 (2001), [arXiv:astro-ph/0108011](#).
- [48] V. Corbin and N. J. Cornish, *Class. Quant. Grav.* **23**, 2435 (2006), [arXiv:gr-qc/0512039](#).

- [49] M. Maggiore, *Phys. Rept.* **331**, 283 (2000), [arXiv:gr-qc/9909001](#).
- [50] L. Pagano, L. Salvati, and A. Melchiorri, *Phys. Lett. B* **760**, 823 (2016), [arXiv:1508.02393 \[astro-ph.CO\]](#).
- [51] P. D. Lasky *et al.*, *Phys. Rev. X* **6**, 011035 (2016), [arXiv:1511.05994 \[astro-ph.CO\]](#).
- [52] P. D. Meerburg, R. Hložek, B. Hadzhiyska, and J. Meyers, *Phys. Rev. D* **91**, 103505 (2015), [arXiv:1502.00302 \[astro-ph.CO\]](#).
- [53] C. Caprini and D. G. Figueroa, *Class. Quant. Grav.* **35**, 163001 (2018), [arXiv:1801.04268 \[astro-ph.CO\]](#).
- [54] T. J. Clarke, E. J. Copeland, and A. Moss, (2020), [arXiv:2004.11396 \[astro-ph.CO\]](#).
- [55] T. Namikawa, S. Saga, D. Yamauchi, and A. Taruya, *Phys. Rev. D* **100**, 021303 (2019), [arXiv:1904.02115 \[astro-ph.CO\]](#).
- [56] P. Adshead, J. T. Giblin, T. R. Scully, and E. I. Sfakianakis, *JCAP* **12**, 034 (2015), [arXiv:1502.06506 \[astro-ph.CO\]](#).
- [57] D. J. E. Marsh, *Phys. Rept.* **643**, 1 (2016), [arXiv:1510.07633 \[astro-ph.CO\]](#).
- [58] U. Seljak, U.-L. Pen, and N. Turok, *Phys. Rev. Lett.* **79**, 1615 (1997), [arXiv:astro-ph/9704231](#).
- [59] B. Salehian, M. A. Gorji, S. Mukohyama, and H. Firouzjahi, (2020), [arXiv:2007.08148 \[hep-ph\]](#).
- [60] J. T. Giblin and E. Thrane, *Phys. Rev. D* **90**, 107502 (2014), [arXiv:1410.4779 \[gr-qc\]](#).
- [61] J. L. Cook and L. Sorbo, *Phys. Rev. D* **85**, 023534 (2012), [Erratum: *Phys.Rev.D* 86, 069901 (2012)], [arXiv:1109.0022 \[astro-ph.CO\]](#).
- [62] N. Barnaby, E. Pajer, and M. Peloso, *Phys. Rev. D* **85**, 023525 (2012), [arXiv:1110.3327 \[astro-ph.CO\]](#).
- [63] M. M. Anber and L. Sorbo, *Phys. Rev. D* **85**, 123537 (2012), [arXiv:1203.5849 \[astro-ph.CO\]](#).
- [64] V. Domcke, M. Pieroni, and P. Binétruy, *JCAP* **06**, 031 (2016), [arXiv:1603.01287 \[astro-ph.CO\]](#).
- [65] N. Bartolo *et al.*, *JCAP* **12**, 026 (2016), [arXiv:1610.06481 \[astro-ph.CO\]](#).
- [66] P. Agrawal, N. Kitajima, M. Reece, T. Sekiguchi, and F. Takahashi, *Phys. Lett. B* **801**, 135136 (2020), [arXiv:1810.07188 \[hep-ph\]](#).
- [67] C. S. Machado, W. Ratzinger, P. Schwaller, and B. A. Stefanek, *JHEP* **01**, 053 (2019), [arXiv:1811.01950 \[hep-ph\]](#).
- [68] C. S. Machado, W. Ratzinger, P. Schwaller, and B. A. Stefanek, (2019), [arXiv:1912.01007 \[hep-ph\]](#).
- [69] M. Bastero-Gil, J. Santiago, L. Ubaldi, and R. Vega-Morales, *JCAP* **04**, 015 (2019), [arXiv:1810.07208 \[hep-ph\]](#).
- [70] R. T. Co, A. Pierce, Z. Zhang, and Y. Zhao, *Phys. Rev. D* **99**, 075002 (2019), [arXiv:1810.07196 \[hep-ph\]](#).
- [71] J. A. Dror, K. Harigaya, and V. Narayan, *Phys. Rev. D* **99**, 035036 (2019), [arXiv:1810.07195 \[hep-ph\]](#).
- [72] M. Zaldarriaga and U. Seljak, *Phys. Rev. D* **55**, 1830 (1997), [arXiv:astro-ph/9609170](#).
- [73] T. Kite, A. Ravenni, S. P. Patil, and J. Chluba, (2020), [arXiv:2010.00040 \[astro-ph.CO\]](#).
- [74] J. Towns, T. Cockerill, M. Dahan, I. Foster, K. Gauthier, A. Grimshaw, V. Hazlewood, S. Lathrop, D. Lifka, G. D. Peterson, R. Roskies, J. R. Scott, and N. Wilkins-Diehr, *Computing in Science & Engineering* **16**, 62 (2014).
- [75] A. Klöckner, N. Pinto, Y. Lee, B. Catanzaro, P. Ivanov, and A. Fasih, *Parallel Computing* **38**, 157 (2012).
- [76] A. Klöckner, in *Proceedings of ARRAY '14: ACM SIGPLAN Workshop on Libraries, Languages, and Compilers for Array Programming* (Association for Computing Machinery, Edinburgh, Scotland., 2014).
- [77] L. Dalcín, R. Paz, M. Storti, and J. D'Elía, *Journal of Parallel and Distributed Computing* **68**, 655 (2008).
- [78] L. Dalcín, R. Paz, and M. Storti, *Journal of Parallel and Distributed Computing* **65**, 1108 (2005).
- [79] Dalcin, Lisandro and Mortensen, Mikael and Keyes, David E, *Journal of Parallel and Distributed Computing* (2019), [10.1016/j.jpdc.2019.02.006](#).
- [80] T. E. Oliphant, *A guide to NumPy*, Vol. 1 (Trelgol Publishing USA, 2006).
- [81] P. Virtanen, R. Gommers, T. E. Oliphant, M. Haberland, T. Reddy, D. Cournapeau, E. Burovski, P. Peterson, W. Weckesser, J. Bright, S. J. van der Walt, M. Brett, J. Wilson, K. Jarrod Millman, N. Mayorov, A. R. J. Nelson, E. Jones, R. Kern, E. Larson, C. Carey, Í. Polat, Y. Feng, E. W. Moore, J. VanderPlas, D. Laxalde, J. Perktold, R. Cimrman, I. Henriksen, E. A. Quintero, C. R. Harris, A. M. Archibald, A. H. Ribeiro, F. Pedregosa, P. van Mulbregt, and S. . . Contributors, *Nature Methods* **17**, 261 (2020).
- [82] L. Husdal, *Galaxies* **4**, 78 (2016), [arXiv:1609.04979 \[astro-ph.CO\]](#).